RSC Advances

PAPER

View Article Online
View Journal | View Issue

Cite this: *RSC Adv.*, 2021, **11**, 34086

Regioselective formylation of rhenium-oxo and gold corroles: substituent effects on optical spectra and redox potentials †

Rune F. Einrem,[a] Einar Torfi Jonsson,[a] Simon J. Teat,[b] Nicholas S. Settineri,[bc] Abraham B. Alemayehu*[a] and Abhik Ghosh*[a]

Received 19th July 2021
Accepted 29th September 2021

DOI: 10.1039/d1ra05525a

rsc.li/rsc-advances

Vilsmeier–Haack formylation of ReO and Au *meso*-triarylcorroles over 16–18 hours affords moderate to good yields (47–65%) of the ReO-3-formyl and Au-3,17-diformyl derivatives in a highly regioselective manner. Formylation was found to effect substantial upshifts for redox potentials (especially the reduction potentials) as well as significant to dramatic redshifts for both the Soret and Q bands.

Introduction

Our research on 5d metallocorroles[1–4] began a decade ago, with two publications documenting the first examples of gold corroles. The first of these reported gold insertion into β-octabromo-*meso*-triarylcorroles,[5] which was also accomplished at about the same time by Gross and coworkers.[6] The second paper described Au insertion into simple *meso*-triarylcorroles with Au(III) acetate[7] – a significant breakthrough, considering the steric mismatch between the large ionic radii of 5d transition metals and the relatively constricted central cavity of corroles. The 'acetate method' has since become the method of choice for the synthesis of Au corroles. Understandably, we were intrigued by the possibility of inserting other heavier transition metals into corroles and, to our satisfaction, the first ^{99}TcO,[8] ReO,[9] ReNAr,[10] RuN,[11] OsN,[12] and Pt[13,14] triarylcorroles (as well as Mo and W biscorroles[15–17] and quadruple-bonded Re corrole dimers[18]) were synthesized in our Tromsø laboratory. Several of the 5d metallocorroles[19–24] were found to exhibit room-temperature NIR phosphorescence, leading to applications as oxygen sensors and as photosensitizers in photodynamic therapy and dye-sensitized solar cells.[25–27] In contrast (compared to 3d metallocorroles,[28,29] especially Cu corroles[30–34]), the chemical reactivity of the 5d complexes remains poorly explored. Peripheral functionalizations accomplished so far include β-perchlorination[35] and perbromination,[36,37] as well as polyiodinations.[38,39] Metal-centered transformations include the generation of Mo and Re Viking-helmet dichlorido derivatives from the corresponding oxido precursors.[40,41] In an alternative approach, the use of water-soluble, axial phosphine ligands has led to water-soluble iridium corroles.[42] A final, more esoteric example consists of the use of an OsN corrole as a π-acceptor ligand in formation of an $Os^{VI}N–Pt^{II}$ heterobimetallic complex.[35] Here we document our efforts to formylate ReO and Au corroles *via* the Vilsmeier–Haack method,[43] which has previously been used for free-base, aluminum and gallium corroles.[44–47] As before, the reaction was found to proceed in a highly regioselective manner, with ReO and Au corroles affording mono- and diformyl derivatives, respectively (Fig. 1). Optical and electrochemical characterization of the products permitted a moderately detailed, experimental picture of the substantial electronic effects of β-formyl groups, as recounted below.

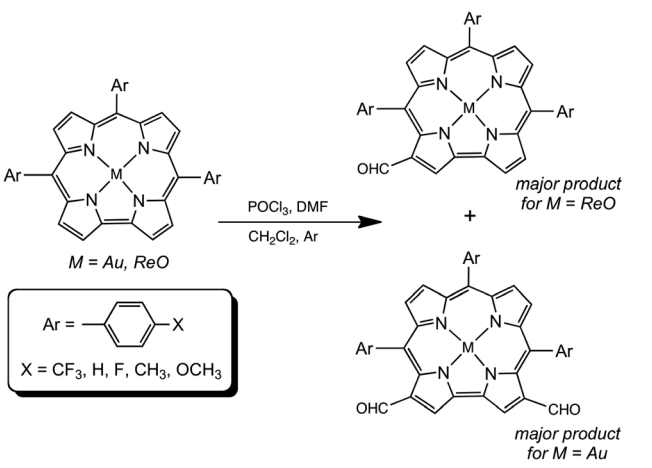

Fig. 1 Formylation of Au and ReO corroles.

[a]*Department of Chemistry, UiT – The Arctic University of Norway, N-9037 Tromsø, Norway. E-mail: abraham.alemayehu@uit.no; abhik.ghosh@uit.no*

[b]*Advanced Light Source, Lawrence Berkeley National Laboratory, Berkeley, CA 94720-8229, USA*

[c]*Department of Chemistry, University of California, Berkeley, Berkeley, California 94720, USA*

† Electronic supplementary information (ESI) available. CCDC 2091847 and 2091848. For ESI and crystallographic data in CIF or other electronic format see DOI: 10.1039/d1ra05525a

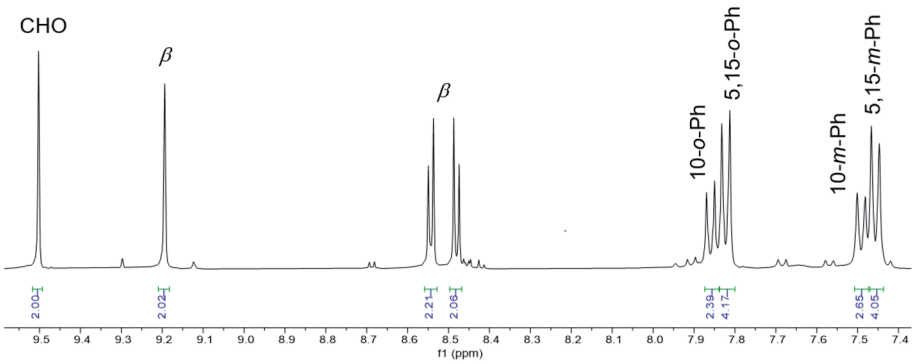

Fig. 2 Aromatic region of the ^{1}H NMR spectrum (400 MHz, $CDCl_3$, 293 K) of Au[T*p*FPC-3,17-$(CHO)_2$].

Results and discussion

(a) Synthesis and proof of composition

Vilsmeier–Haack formylation, carried out over 16–18 h at 0 °C to room temperature, proceeded smoothly for both ReO and Au *meso*-tris(*para*-X-phenyl)corroles, M[T*p*XPC] (M = ReO, Au), regioselectively affording good yields of the 3-monoformyl (~50%) and 3,17-diformyl (~60%) derivatives for the two metals, respectively. The major products, hereafter denoted as Re[T*p*XPC-3-CHO](O) and Au[T*p*XPC-3,17-$(CHO)_2$], were fully characterized and the regiochemistry of formylation was established largely *via* ^{1}H NMR spectroscopy. In particular, the simplicity of the ^{1}H NMR of the Au-diformyl derivatives (relative to the ReO-monoformyl derivatives) immediately suggested a regiochemistry consistent with time-averaged C_{2v} symmetry (Fig. 2 and 3). The minor products – the ReO-diformyl and Au-monoformyl derivatives – generally could not be fully characterized. Surprisingly, two minor products – Re[T*p*CH_3PC-3,17-$(CHO)_2$](O) and Au[T*p*CH_3PC-3-CHO] – proved amenable to single-crystal X-ray structure determination (Table 1 and Fig. 4 and 5). The structures established that the formyl groups are essentially coplanar with the mean plane of the pyrrole rings they are attached to, but aside from that, they proved largely unremarkable. Finally, in a brief examination of their reactivity, ReO 3-formylcorroles were found to undergo facile Knoevenagel condensation with active methylene compounds (Fig. 6). While

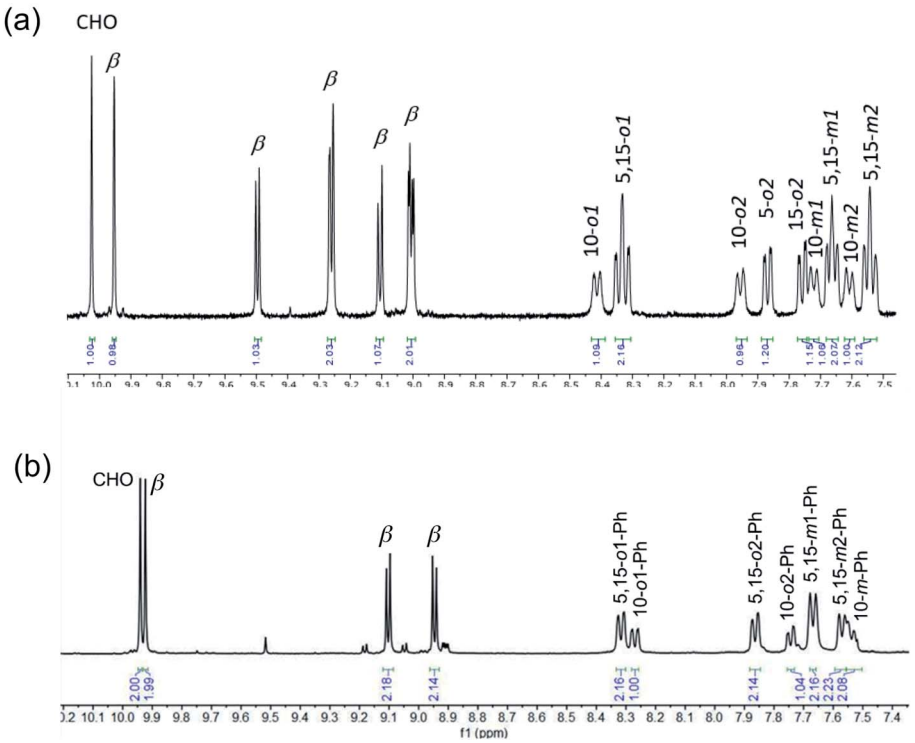

Fig. 3 Aromatic region of the ^{1}H NMR spectra (400 MHz, $CDCl_3$, 273 K) of (a) Re[T*p*CH_3PC-3-CHO](O) and (b) Re[T*p*CH_3PC-3-17-$(CHO)_2$](O). Note the different numbers of β protons in the two complexes. Note also that the most downfield singlet has been tacitly assigned as the formyl proton.

Table 1 Selected crystallographic data for the complexes analyzed

	Re[T*p*CH$_3$PC-3,17-(CHO)$_2$](O)	Au[T*p*FPC-3-CHO]
Chemical formula	$C_{45}H_{36}N_4O_3Re$	$C_{38}H_{20}F_3N_4OAu$
Formula mass	866.98	802.55
Crystal system	Triclinic	Monoclinic
Crystal size (mm^3)	0.230 × 0.080 × 0.020	0.100 × 0.020 × 0.010
Space group	$P\bar{1}$	$C2/c$
λ (Å)	0.7288	0.7288
a (Å)	9.5807(4)	20.9037(12)
b (Å)	12.6649(6)	19.7169(12)
c (Å)	29.1467(13)	15.8376(10)
α (deg)	95.279(2)	90
β (deg)	91.627(2)	91.467(3)
γ (deg)	90.341(2)	90
Z	4	8
V (Å^3)	3520.1(3)	6525.4(7)
Temperature (K)	100(2)	100(2)
Density (g cm^{-3})	1.636	1.634
Measured reflections	131 064	84 580
Unique reflections	21 566	10 078
Parameters	975	424
Restraints	40	0
R_{int}	0.0354	0.0697
θ Range (deg.)	1.744–31.439	2.913–31.600
R_1, wR_2 all data	0.0361, 0.0667	0.0453, 0.1001
S (GooF) all data	1.092	1.070
Max/min res. dens. (e Å^{-3})	2.379/−2.218	1.925/−1.512

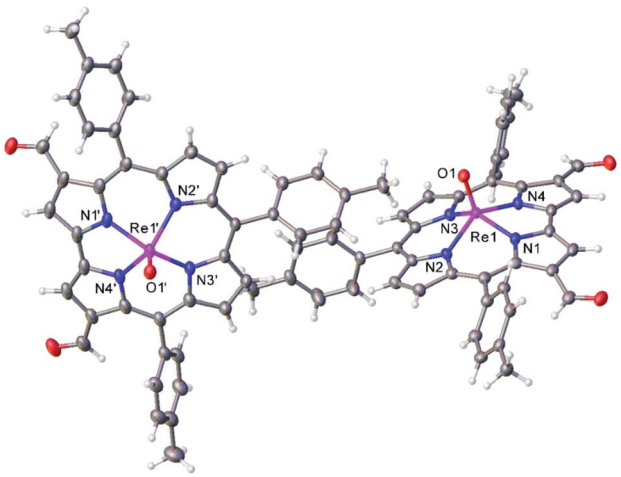

Fig. 4 Thermal ellipsoid plot for Re[T*p*CH$_3$PC-3,17-(CHO)$_2$](O). Selected distances (Å): Re1–N1 2.007(2), Re1–N2 2.012(2), Re1–N3 2.013(2), Re1–N4 1.999(2), and Re1–O1 1.681(2), Re1′–N1′ 1.999(2), Re1′–N2′ 2.016(2), Re1′–N3′ 2.013(2), Re1′–N4′ 2.000(2), Re1′–O1′ 1.685.

a full exposition of reactivity studies is outside the scope of the present study, a few examples of protocols involving cyanoacetic acid are given in the experimental section.

(b) Electronic absorption spectra and redox potentials

Formylation engenders significant redshifts for both the Soret bands and double-humped Q bands of the ReO and Au corroles (Table 2, Fig. 7 and 8). Thus, 3-monoformylation redshifts the Soret maxima by about 8 nm (for either metal), while diformylation brings about redshifts about one-and-a-half (for ReO) to twice (for Au) that magnitude. For the lowest-energy Q bands (for either metal), mono- and diformylation result in redshifts of 20–25 and 37–41 nm, respectively. Interestingly, formylation appears to weaken the intensity of the Soret band, suggesting a certain weakening of macrocyclic aromaticity, while strengthening the Q band, potentially indicating corrole to formyl charge transfer character for the latter feature.

Formylation has a substantial impact on the redox potentials of both ReO and Au corroles (which all correspond to ligand-centered processes[1,3,7,9,48]), the impact on reduction potentials being particularly dramatic (Table 2). Thus, 3-formylation upshifts oxidation potentials of ReO triarylcorroles by 100–170 mV and the reduction potentials by ∼300 mV (Fig. 9). Likewise, 3,17-diformylation upshifts oxidation potentials of Au triarylcorroles by ∼260 mV and the reduction potentials by 500–650 mV (Fig. 10). The larger shifts for the reduction potentials may be qualitatively understood in terms of the ability of the strongly electron-withdrawing formyl substituents to stabilize a negative charge. The effect also translates to smaller electrochemical HOMO–LUMO gaps (*i.e.*, the algebraic difference between the first oxidation and reduction potentials) for the formylated metallocorroles relative to their β-unsubstituted counterparts. For one of the Au corroles, Au[T*p*FPC], we were able to determine the effect of both mono- and diformylation. For both oxidation and reduction potentials, the second formyl group was found to have a distinctly smaller effect relative to the first one – *i.e.*, a nonadditive effect (Fig. 11).

The redox potentials of the compounds studied also provide a potential explanation for the observed tendency toward

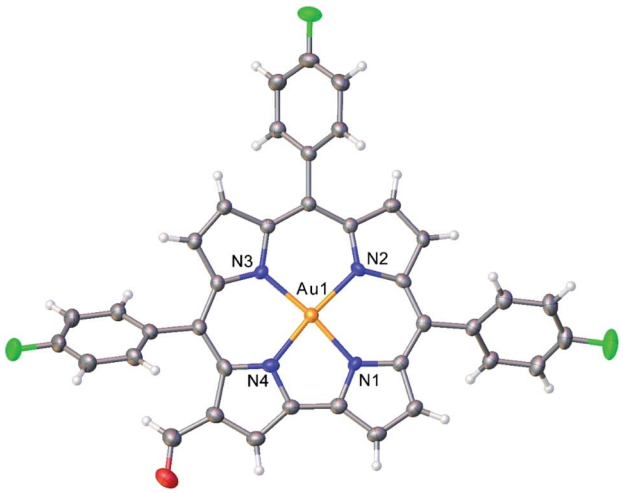

Fig. 5 Thermal ellipsoid plot for Au[T*p*FPC-3-CHO]. Selected distances (Å): Au1–N1 1.939, Au1–N2 1.973, Au1–N3 1.958, Au1–N4 1.950.

monoformylation for ReO corroles and toward diformylation for Au corroles. The oxidation potentials of β-unsubstituted Au triarylcorroles are about 200 mV lower than those of analogous ReO complexes, suggesting that the former are more nucleophilic. (It may be noted that the higher oxidation potentials in the Re case correlates with the higher oxidation state of the Re center, +V, compared to +III for Au. A similar metal oxidation state dependence has long been known for metalloporphyrins.[49]) Moreover, the oxidation potentials of the ReO–monoformyl complexes are about the same as those of analogous Au-diformyl complexes, potentially explaining why formylation stops at the monoformyl stage for ReO triarylcorroles.

Conclusion

Vilsmeier–Haack formylation has been found to proceed in a highly regioselective manner for ReO and Au triarylcorroles, affording 3-formyl and 3,17-diformyl derivatives, respectively, as the major products. The difference in reactivity between the two metals appears at least partially attributable to a difference in oxidation potential, and hence nucleophilicity, between the two families of 5d metallocorroles. The formyl groups engender significant to dramatic redshifts of the Soret and Q bands and large upshifts for the redox potentials for both series of metallocorroles. A preliminary study demonstrating successful Knoevenagel condensations suggests that the formylated products should serve as versatile starting materials for a wide range of functionalized, potentially water-soluble 5d metallocorroles.

Experimental section

Materials and instruments

Except for solvents, all chemicals were obtained from Sigma-Aldrich and used as such. Dichloromethane used in syntheses was dried over 3 Å molecular sieves. CHROMASOLV HPLC-grade *n*-hexane and dichloromethane were used for column chromatography. Silica gel 60 (0.04–0.063 mm particle size; 230–400 mesh, Sigma) was used for column chromatography, with columns about 8 cm in height and 3 cm in diameter. UV-vis spectra were recorded on an HP 8454 spectrophotometer at room temperature. High-resolution electrospray ionization (ESI) mass spectra were recorded on an LTQ Orbitrap XL spectrometer. ^{1}H NMR spectra were recorded on a Bruker Avance III HD 400 MHz spectrometer. Cyclic voltammetry analyses were carried out in dry dichloromethane containing 0.1 M TBAP as a supporting electrolyte. An EG&G 263A potentiostat with a standard three-electrode set-up, consisting of a glassy carbon working electrode (3 mm i.d.), a platinum wire counter electrode, and saturated calomel reference electrode (SCE), was used for cyclic voltammetry.

General procedure for formylation of Re^{V}O triarylcorroles

To a 50 mL round-bottom flask equipped with a magnetic stir-bar, a rubber septum, and an argon in/outlet, and placed in an ice/water bath, were added dichloromethane (5.0 mL), $POCl_3$ (20 mmol, 1.8 mL), and DMF (23 mmol, 1.8 mL) were added. The metallocorrole[7,9] starting material (0.075 mmol, ∼55 mg) was dissolved in dichloromethane (10 mL) and added *via* syringe to the chilled solution. The mixture was left to stir under a constant flow of argon at 0 °C for 15 minutes, whereupon it was allowed to warm to room temperature and left to stir overnight. The following morning, the reaction was quenched with water (3 × 100 mL). The organic phase was dried and subjected to column chromatography on silica gel with 3 : 1 *n*-

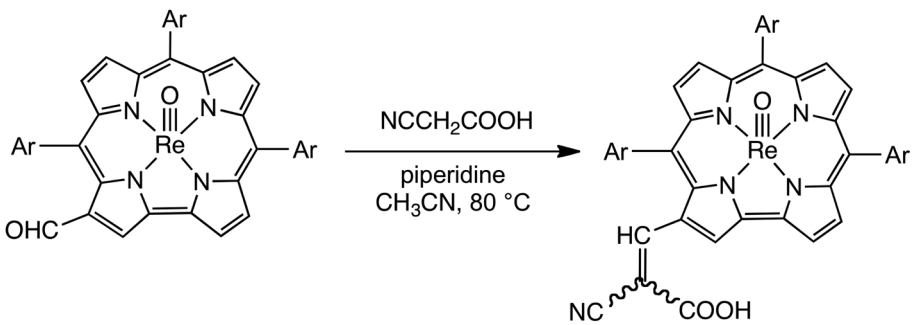

Fig. 6 Knoevenagel condensation of ReO 3-formylcorroles with cyanoacetic acid.

Table 2 UV-vis absorption maxima (nm), redox potentials (V) and electrochemical HOMO–LUMO gaps (Δ*E*, V) for selected compounds

Compound	Soret	Q	$E_{1/2-ox2}$	$E_{1/2-ox1}$	$E_{1/2-red1}$	$E_{1/2-red2}$	Δ*E*	Ref.
Au[T*p*OCH$_3$PC]	420	560, **580**	1.32	0.76	−1.57	—	2.33	6
Au[T*p*CH$_3$PC]	420	560, **576**	1.35	0.78	−1.42	—	2.20	6
Au[TPC]	418	560, **575**	1.35	0.80	−1.38	—	2.18	6
Au[T*p*FPC]	419	559, **573**	1.38	0.85	−1.37	—	2.22	6
Au[T*p*CH$_3$PC-3-CHO]	428	581, 602	—	—	—	—	—	tw
Au[T*p*FPC-3-CHO]	427	580, 597	—	1.03	−1.02	−1.46	2.05	tw
Au[T*p*OCH$_3$PC-3,17-(CHO)$_2$]	439	597, 618	1.36	1.03	−0.92	−1.42	1.95	tw
Au[T*p*CH$_3$PC-3,17-(CHO)$_2$]	439	596, 615	—	1.07	−0.92	−1.43	1.99	tw
Au[TPC-3,17-(CHO)$_2$]	437	596, 611	—	1.14	−0.87	−1.39	2.01	tw
Au[T*p*FPC-3,17-(CHO)$_2$]	436	597, 609	—	1.20	−0.81	−1.34	2.01	tw
Re[T*p*OCH$_3$PC](O)	441	556, **592**	—	0.93	−1.29	—	2.22	8
Re[T*p*CH$_3$PC](O)	440	555, **587**	—	0.94	−1.29	—	2.23	8
Re[TPC](O)	439	552, **585**	—	0.98	−1.26	—	2.24	8
Re[T*p*FPC](O)	438	553, **585**	—	1.01	−1.23	—	2.24	8
Re[T*p*CF$_3$PC](O)	438	552, **585**	—	1.10	−1.16	—	2.26	8
Re[T*p*OCH$_3$PC-3-CHO](O)	449	609	1.30	1.03	−1.00	−1.40	2.03	tw
Re[T*p*CH$_3$PC-3-CHO](O)	449	611	1.41	1.08	−0.96	−1.36	2.04	tw
Re[TPC-3-CHO](O)	452	613	—	1.15	−0.89	−1.29	2.04	tw
Re[T*p*FPC-3-CHO](O)	448	608	—	1.17	−0.90	−1,30	2.07	tw
Re[T*p*CF$_3$PC-3-CHO](O)	448	607	—	1.23	−0.84	−1,25	2.07	tw

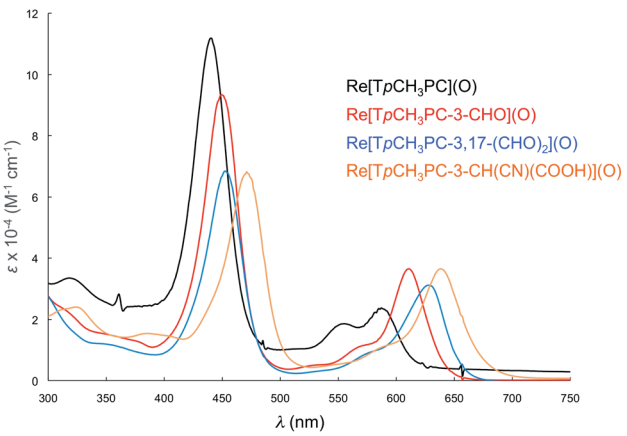

Fig. 7 Comparative UV-vis spectra in dichloromethane for Re[T*p*CH$_3$PC](O) (black), Re[T*p*CH$_3$PC-3-CHO](O) (red), (c) Re[T*p*CH$_3$PC-3,17-(CHO)$_2$](O) (blue), (d) Re[T*p*CH$_3$PC-3-CH(CN)(COOH)](O) (saffron).

hexane/dichloromethane as eluent. Further elution with dichloromethane with up to 0–5% methanol led to product isolation.

Re[TPC-3-CHO](O). Yield 34.5 mg (62.8%). UV-vis (CH_2Cl_2) λ_{max} [nm, $\varepsilon \times 10^{-4}$ (M^{-1} cm^{-1})]: 449 (8.47), 609 (3.19). ^{1}H NMR (400 MHz, 20 °C) δ: 10.06 (s, 1H, CHO); 9.96 (s, 1H, β-H); 9.52 (d, 1H, $^3J_{HH}$ = 4.4 Hz, β-H); 9.25 (d overlapping, 2H, $^3J_{HH}$ = 4.3 Hz, β-H); 9.09 (d, 1H, $^3J_{HH}$ = 5.0 Hz, β-H); 9.00 (d overlapping, 2H, $^3J_{HH}$ = 4.9 Hz, β-H); 8.55 (d, 1H, $^3J_{HH}$ = 7.6 Hz, 10-*o*1-Ph); 8.45 (d overlapping, 2H, $^3J_{HH}$ = 8.2 Hz, 5,15-*o*1-Ph); 8.07 (d, 1H, $^3J_{HH}$ = 6.6 Hz, 10-*o*2-Ph); 7.99 (d, 2H, $^3J_{HH}$ = 7.6 Hz, 5/15-*o*2-Ph); 7.82 (m, 10H, 5/15-*o*2-Ph + 5,10,15-*m*-Ph + 5,10,15-*p*-Ph). MS (ESI): M^+ = 754.1383 (expt), 754.1375 (calcd for $C_{38}H_{23}N_4O_2Re$). Elemental analysis (%) calcd for $C_{38}H_{23}N_4O_2Re$: C 60.55, H 3.08, N 7.43, found C 60.93, H 3.36, N 7.59. IR ν_{ReO}: 992 cm^{-1}, ν_{CHO}: 1659 cm^{-1}

Re[T*p*CH$_3$PC-3-CHO](O). Yield 31.1 mg (56.6%). UV-vis (CH_2Cl_2) λ_{max} [nm, $\varepsilon \times 10^{-4}$ (M^{-1} cm^{-1})]: 449 (9.34), 611 (3.65). ^{1}H NMR (400 MHz, 0 °C) δ: 10.03 (s, 1H, CHO); 9.95 (s, 1H, β-H); 9.50 (d, 1H, $^3J_{HH}$ = 4.4 Hz, β-H); 9.26 (d, 2H, $^3J_{HH}$ = 4.5 Hz, β-H); 9.11 (d, 1H, $^3J_{HH}$ = 5.1 Hz, β-H); 9.01 (dd, 2H, $^3J_{HH}$ = 4.9, 1.9 Hz, β-H); 8.41 (d, 1H, $^3J_{HH}$ = 7.5 Hz, 10-*o*1-Ph); 8.33 (t, 2H, $^3J_{HH}$ = 9.3 Hz, 5,15-*o*1-Ph); 7.96 (d, 1H, $^3J_{HH}$ = 7.5 Hz, 10-*o*2-Ph); 7.87 (d, 1H, $^3J_{HH}$ = 7.6 Hz, 5/15-*o*2-Ph); 7.76 (d, 1H, $^3J_{HH}$ = 6.7 Hz, 5/15-*o*1-Ph); 7.72 (d, 1H, $^3J_{HH}$ = 7.7 Hz, 10-*m*1-Ph); 7.66 (t, 2H, $^3J_{HH}$ = 6.7 Hz, 5,15-*m*1-Ph); 7.61 (d, 1H, $^3J_{HH}$ = 7.7 Hz, 10-*m*2-Ph); 7.54 (t, 2H, $^3J_{HH}$ = 7.5 Hz, 5,15-*m*2-Ph); 2.72 (s, 3H, 10-*p*-CH$_3$); 2.70 (s, 6H, 5,15-*p*-CH$_3$). MS (ESI): M^+ = 796.1853 (expt), 796.1845 (calcd for $C_{41}H_{29}N_4O_2Re$). Elemental analysis (%) calcd for $C_{41}H_{29}N_4O_2Re$: C 61.87, H 3.67, N 7.04; found C 61.63, H 3.62, N 7.34. IR (cm^{-1}): ν_{ReO} 992, ν_{CHO} 1659.

Re[T*p*OCH$_3$PC-3-CHO](O). Yield 36 mg (65.4%). UV-vis (CH_2Cl_2) λ_{max} [nm, $\varepsilon \times 10^{-4}$ (M^{-1} cm^{-1})]: 452 (11.06), 613 (4.14). ^{1}H NMR (400 MHz, −20 °C, dichloromethane-d2) δ: 9.97 (s, 1H, CHO); 9.93 (s, 1H, β-H); 9.50 (d, 1H, $^3J_{HH}$ = 4.4 Hz, β-H); 9.32 (d, 1H, $^3J_{HH}$ = 4.9 Hz, β-H); 9.25 (d, 1H, $^3J_{HH}$ = 4.4 Hz, β-H); 9.15 (d, 1H, $^3J_{HH}$ = 5.0 Hz, β-H); 9.06 (t, 2H, $^3J_{HH}$ = 4.3 Hz, β-H); 8.44 (d, 1H, $^3J_{HH}$ = 6.5 Hz, 10-*o*1-Ph); 8.34 (d, 2H, $^3J_{HH}$ = 8.3 Hz, 5,15-*o*1-Ph); 8.02 (d, 1H, $^3J_{HH}$ = 6.6 Hz, 10-*o*2-Ph); 7.89 (d, 1H, $^3J_{HH}$ = 6.2 Hz, 5/15-*o*2-Ph); 7.82 (d, 1H, $^3J_{HH}$ = 6.2 Hz, 5/15-*o*2-Ph); 7.43 (d, 1H, $^3J_{HH}$ = 5.9 Hz, 10-*m*1-Ph); 7.39–7.31 (m, 3H, 10-*m*2-Ph & 5,15-*m*1-Ph); 7.27–7.23 (m, 2H, 5,15-*m*2-Ph); 4.06 (s, 6H, 5,15-*p*-OCH$_3$); 4.04 (s, 3H, 10-*p*-OCH$_3$). MS (ESI): M^+ = 844.1695 (expt), 844.1692 (calcd for $C_{41}H_{29}N_4O_5Re$). Elemental analysis (%) calcd for $C_{41}H_{29}N_4O_5Re$: C 58.35, H 3.46, N 6.64; found C 58.13, H 3.62, N 6.54. IR (cm^{-1}): ν_{ReO} 992, ν_{CHO} 1655.

Re[T*p*FPC-3-CHO](O). Yield 35 mg (63.8%). UV-vis (CH_2Cl_2) λ_{max} [nm, $\varepsilon \times 10^{-4}$ (M^{-1} cm^{-1})]: 448 (8.87), 608 (2.93). ^{1}H NMR

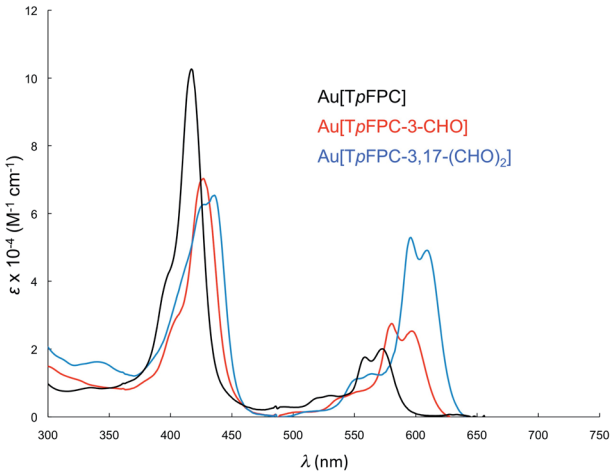

Fig. 8 Comparative UV-vis spectra in dichloromethane for Au[T*p*FPC] (black), Au[T*p*FPC-3-CHO] (red), (c) Au[T*p*FPC-3,17-$(CHO)_2$] (blue).

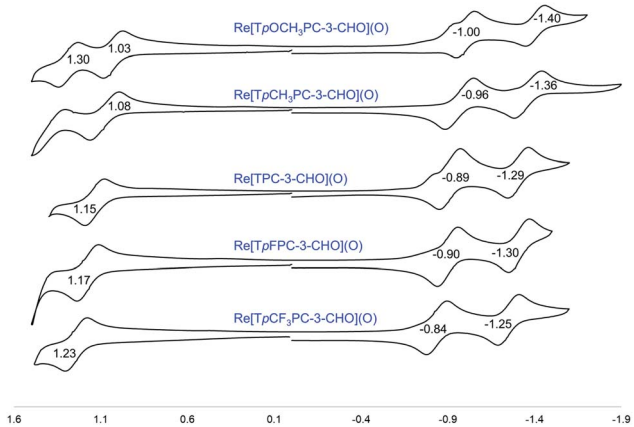

Fig. 9 Cyclic voltammograms (V *vs.* SCE) for Re[T*p*XPC-3-CHO](O) derivatives in dichloromethane containing 0.1 M TBAP.

(400 MHz, $CDCl_3$, 20 °C) δ: 10.07 (s, 1H, CHO); 10.05 (s, 1H, β-H); 9.52 (d, 1H, $^3J_{HH} = 4.4$ Hz, β-H); 9.22 (d, 1H, $^3J_{HH} = 4.4$ Hz, β-H); 9.21 (d, 1H, $^3J_{HH} = 4.9$ Hz, β-H); 9.06 (d, 1H, $^3J_{HH} = 5.0$ Hz, β-H); 8.975 (d, 1H, $^3J_{HH} = 4.9$ Hz, β-H); 8.972 (d, 1H, $^3J_{HH} = 5.1$ Hz, β-H); 8.46–8.38 (m, 3H, Ph-H); 7.93 (m, 2H, Ph-H); 7.81 (m, 2H, Ph-H); 7.54–7.59 (m, 3H, Ph-H); 7.42–7.59 (m, 2H, Ph-H). MS (ESI): M^+ = 808.1107 (expt), 808.1103 (calcd for $C_{38}H_{20}F_3N_4O_2Re$). Elemental analysis (%) calcd for $C_{38}H_{20}F_3N_4O_2Re$: C 56.50, H 2.50, N 6.94; found C 56.23, H 2.62, N 6.63 IR ν_{ReO}: 1007 cm^{-1}, ν_{CHO}: 1730, 1666 cm^{-1}.

Re[T*p*CF_3PC-3-CHO](O). Yield 25 mg (47.6%). UV-vis (CH_2Cl_2) λ_{max} [nm, $\varepsilon \times 10^{-4}$ (M^{-1} cm^{-1})]: 448 (9.21), 607 (3.17). ^{1}H NMR (400 MHz, −20 °C, $CDCl_3$) δ: 10.14 (s, 1H, CHO); 9.99 (s, 1H, β-H); 9.61 (d, 1H, $^3J_{HH} = 4.4$ Hz, β-H); 9.27 (dd, 2H, $^3J_{HH} = 9.4, 4.7$ Hz, β-H); 9.06 (d, 1H, $^3J_{HH} = 5.1$ Hz, β-H); 9.01 (dd overlapping, 2H, $^3J_{HH} = 4.9, 3.4$ Hz, β-H); 8.68 (d, 1H, $^3J_{HH} = 8.0$ Hz, 10-*m*1-Ph); 8.63 (dd overlapping, 2H, $^3J_{HH} = 12.0, 8.1$ Hz, 5,15-*m*1-Ph); 8.22–8.14 (m, 5H, 10-*m*2-Ph & 5,15-*m*2-Ph & 10-*o*-Ph); 8.10–8.00 (m, 4H, 5,15-*o*-Ph). MS (ESI): M^- = 958.1015 (expt), 958.1008 (calcd for $C_{41}H_{20}F_9N_4O_2Re$). Elemental analysis (%) calcd for $C_{41}H_{20}F_9N_4O_2Re$: C 51.41, H 2.10, N 5.85; found C 51.13, H 2.32, N 5.54. IR ν_{ReO}: 992 cm^{-1}, ν_{CHO}: 1663 cm^{-1}.

Re[T*p*CH_3PC-3,17-$(CHO)_2$](O). Small quantities of this minor product were combined from multiple syntheses to derive the following spectroscopic data. UV-vis (CH_2Cl_2) λ_{max} [nm, $\varepsilon \times 10^{-4}$ (M^{-1} cm^{-1})]: 452 (6.84), 628 (3.12). ^{1}H NMR (400 MHz, −20 °C, $CDCl_3$) δ: 9.94 (s, 2H, CHO); 9.92 (s, 2H, β-H); 9.10 (d, 2H, $^3J_{HH} = 5.0$ Hz, β-H); 8.95 (d, 2H, $^3J_{HH} = 5.0$ Hz, β-H); 8.32 (d, 2H, $^3J_{HH} = 8.6$ Hz, 5,15-*o*1-Ph); 8.27 (d, 1H, $^3J_{HH} = 7.7$ Hz, 10-*o*1-Ph); 7.86 (d, 2H, $^3J_{HH} = 8.8$ Hz, 5,15-*o*2-Ph); 7.74 (d, 1H, $^3J_{HH} = 7.6$ Hz, 10-*o*2-Ph); 7.67 (d, 2H, $^3J_{HH} = 7.7$ Hz, 5,15-*m*1-Ph); 7.57 (d, 2H, $^3J_{HH} = 7.6$ Hz, 5,15-*m*2-Ph); 7.99 (d, 2H, $^3J_{HH} = 8.0$ Hz, 10-*m*-Ph); 2.71 (s, 6H, 5,15-*p*-CH_3); 2.70 (s, 3H, 10-*p*-CH_3). MS (ESI): M^+ = 824.1807 (expt), 824.1792 (calcd for $C_{42}H_{29}N_4O_3Re$).

General synthesis of cyanoacetic-acid (Knoevenagel) adducts

To a two-necked 50 mL round-bottom flask equipped with a rubber septum, a reflux condenser, a magnetic stir-bar, and an argon inlet/outlet, was added the desired Re^VO-corrole-3-CHO derivative (0.04 mmol, ∼30 mg), dissolved in acetonitrile (10 mL). To this solution, cyanoacetic acid (30 mg, 0.04 mmol) and piperidine (two drops) were added. The reaction mixture was heated to reflux (∼80 °C) and left to stir for ∼1 hour under argon. After cooling, the reaction was quenched by washing with water (3 × 100 mL), prior to purification *via* column chromatography on silica gel using dichloromethane with 5% methanol as mobile phase. Unreacted monoformyl starting material eluted first, followed by the desired product.

Re[TPC-3-CH(CN)(CO_2H)](O). Yield 21 mg (64.3%). UV-vis (CH_2Cl_2) λ_{max} [nm, $\varepsilon \times 10^{-4}$ (M^{-1} cm^{-1})]: 470 (7.32), 637 (3.98). ^{1}H NMR (400 MHz, −20 °C) δ: 10.62 (s, 1H, β-H); 9.54 (d, 1H, $^3J_{HH} = 4.4$ Hz, β-H); 9.25 (d, 1H, $^3J_{HH} = 4.4$ Hz, β-H); 9.22 (d, 1H, $^3J_{HH} = 4.9$ Hz, β-H); 9.00 (d, 1H, $^3J_{HH} = 5.0$ Hz, β-H); 8.96 (d, 2H, $^3J_{HH} = 4.5$ Hz, β-H); 8.75 (s, 1H, C–H); 8.53 (d, 1H, $^3J_{HH} = 7.4$ Hz, 10-*o*1-Ph); 8.42 (t, 2H, $^3J_{HH} = 8.6$ Hz, 5,15-*o*1-Ph); 8.06 (d, 1H, $^3J_{HH} = 6.7$ Hz, 10-*m*1-Ph); 7.86 (m, 10H, 10-*o*2/*m*2/*p*-Ph, 5,15-*o*2/*m*/*p*-Ph). MS (ESI): M^+ = 821.1360 (expt), 821.1366 (calcd for $C_{41}H_{24}N_5O_3Re$). Elemental analysis (%) calcd for $C_{41}H_{24}N_5O_3Re$: C 59.99, H 2.95, N 8.53; found C 59.73, H 2.62, N 8.59. IR (cm^{-1}): ν_{ReO} 996, ν_{CHO} 1570 cm^{-1}, ν_{CN}: 1704 cm^{-1}.

Re[T*p*CH_3PC-3-CH(CN)(CO_2H)](O). Yield 23.9 mg (79.74%). UV-vis (CH_2Cl_2) λ_{max} [nm, $\varepsilon \times 10^{-4}$ (M^{-1} cm^{-1})]: 471 (6.82), 638 (3.65). ^{1}H NMR (400 MHz, 0 °C) δ: 10.58 (s, 1H, β-H); 9.52 (d, 1H, $^3J_{HH} = 4.6$ Hz, β-H); 9.23 (dd, 2H, $^3J_{HH} = 6.8, 4.6$ Hz, β-H); 9.03 (d, 1H, $^3J_{HH} = 4.8$ Hz, β-H); 8.96 (d, 2H, $^3J_{HH} = 5.1$ Hz, β-H); 8.73 (s, 1H, CH); 8.40 (d, 1H, $^3J_{HH} = 7.6$ Hz, 10-*o*1-Ph); 8.30 (d, 1H, $^3J_{HH} = 7.8$ Hz, 5/15-*o*1-Ph); 8.26 (d, 1H, $^3J_{HH} = 7.8$ Hz, 5/15-*o*1-Ph); 7.96 (d, 1H, $^3J_{HH} = 7.4$ Hz, 10-*o*2-Ph); 7.83 (d, 1H, $^3J_{HH} = 8.1$ Hz, 10-*m*1-Ph); 7.74 (t, 3H, $^3J_{HH} = 8.7$ Hz, 10-*m*2-Ph & 5,15-*o*2-Ph); 7.69–7.59 (m, 3H, 5,15-*m*1-Ph & 5/15-*m*2-Ph); 7.55 (d, 1H, $^3J_{HH} = 7.7$ Hz, 5/15-*m*2-Ph); 2.80 (s, 3H, 10-*p*-CH_3); 2.71 (s, 6H, 5,15-*p*-CH_3). MS (ESI): M^+ = 863.1831 (expt), 863.1836 (calcd for $C_{44}H_{30}N_5O_3Re$). Elemental analysis (%) calcd for $C_{44}H_{30}N_5O_3Re$: C 61.24, H 3.50, N 8.12; found C 61.13, H 3.62, N 8.54.

Re[TpFPC-CH(CN)(CO_2H)](O). Yield 19.7 mg (66.2%). UV-vis (CH_2Cl_2) λ_{max} [nm, $\varepsilon \times 10^{-4}$ (M^{-1} cm^{-1})]: 470 (4.31), 637 (2.19).

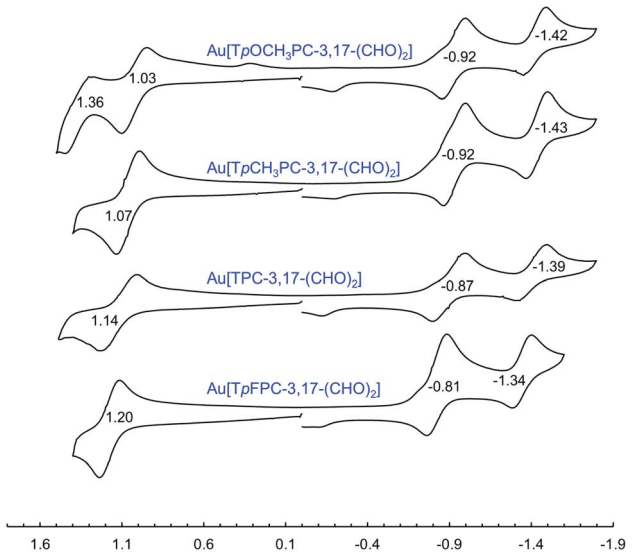

Fig. 10 Cyclic voltammograms (V *vs.* SCE) for Au[T*p*XPC-3,17-(CHO)$_2$] derivatives in dichloromethane containing 0.1 M TBAP.

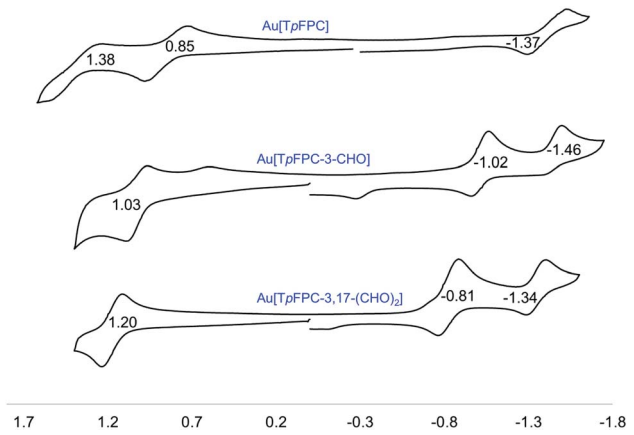

Fig. 11 Cyclic voltammograms (V *vs.* SCE) for Au[T*p*XPC-(CHO)$_n$] (n = 0, 1, 2) derivatives in dichloromethane containing 0.1 M TBAP.

^{1}H NMR (400 MHz, THF, 20 °C) δ: 10.63 (s, 1H, β-H); 9.79 (d, 1H, $^3J_{HH}$ = 4.4 Hz, β-H); 9.29 (dd, 2H, $^3J_{HH}$ = 4.68, 2.4 Hz, β-H); 9.09 (d, 1H, $^3J_{HH}$ = 5.0 Hz, β-H); 9.03 (dd, 2H, $^3J_{HH}$ = 7.0, 5.0 Hz, β-H); 8.66 (s, 1H, CH); 8.50 (ddd, 1H, $^3J_{HH}$ = 8.1, 5.4, 2.3 Hz, 10-*m*1-Ph); 8.43 (ddd, 1H, $^3J_{HH}$ = 8.1, 5.4, 2.3 Hz, 5/15-*m*1-Ph); 7.97–7.86 (m, 3H, 5/15-*m*1-Ph, 10-*m*2, *o*1-Ph); 7.74–7.48 (m, 7H, Ph-H). MS (ESI): M$^+$ 875.1163 (expt), 875.1163 (calcd for $C_{41}H_{21}F_3N_5O_3Re$). Elemental analysis (%) calcd for $C_{41}H_{21}F_3N_5O_3Re$: C 56.29, H 2.42, N 8.01; found C 56.13, H 2.62, N 8.34. IR ν_{ReO}: 996 cm^{-1}, ν_{CHO}: 1328 cm^{-1}.

Re[TpCF$_3$PC-CH(CN)(CO$_2$H)](O). Yield 11 mg (46.7%). UV-vis (CH_2Cl_2) λ_{max} [nm, $\varepsilon \times 10^{-4}$ (M^{-1} cm^{-1})]: 466 (8.45), 631 (4.36). ^{1}H NMR (400 MHz, $CDCl_3$, 20 °C) δ: 10.58 (s, 1H, β-H); 9.55 (d, 1H, $^3J_{HH}$ = 4.6 Hz, β-H); 9.18 (d, 1H, $^3J_{HH}$ = 4.7 Hz, β-H); 9.13 (d, 1H, $^3J_{HH}$ = 4.7 Hz, β-H); 8.93 (d, 1H, $^3J_{HH}$ = 5.0, β-H); 8.90–8.86 (m, 2H, β-H); 8.52–8.46 (m, 4H, *m*1-Ph + CH); 8.11 (dd, 4H, $^3J_{HH}$ = 12.4, 8.8 Hz, 5,10,15-*m*2-Ph/10-*o*1-Ph); 8.02 (s broad, 3H, 10-*o*2-Ph/5,15-*o*1-Ph); 7.95 (d, 2H, $^3J_{HH}$ = 3.8 Hz, 5,15-*o*2-Ph). MS (ESI): M$^-$ 1025.1069 (expt), 1025.1064 (calcd for $C_{44}H_{21}F_9N_5O_3Re$). Elemental analysis (%) calcd for $C_{44}H_{21}F_9N_5O_3Re$: C 51.57, H 2.07, N 6.83; found C 51.33, H 2.32, N 6.54. IR ν_{ReO}: 996 cm^{-1}, ν_{CHO}: 1328 cm^{-1}.

General procedure for formylation of Au triarylcorroles

To a 50 mL round-bottom flask equipped with a magnetic stir-bar, a rubber septum, and an argon inlet/outlet and placed in an ice/water bath, were added dichloromethane (5 mL), $POCl_3$ (20 mmol, 1.8 mL), and DMF (23 mmol, 1.8 mL). Metallocorrole (0.025 mmol, ~20 mg) was dissolved in DCM (10 mL) and added *via* syringe to the cold solution. The mixture was left to stir under a constant flow of argon at 0 °C for 15 minutes upon heating to room temperature. The reaction was left to stir overnight. The following morning the reaction was quenched *via* washing with water (3 × 100 mL) before purification through silica gel column chromatography using a mixture of *n*-hexane/dichloromethane (3 : 1) as eluent to isolate any unreacted starting material. The desired product was isolated by further elution with dichloromethane or a mixture with dichloromethane and methanol (5%).

Au[TPC-3,17-(CHO)$_2$]. Yield 20 mg (61.17%). UV-vis (CH_2Cl_2) λ_{max} [nm, $\varepsilon \times 10^{-4}$ (M^{-1} cm^{-1})]: 426 (7.53), 437 (8.33), 596 (6.78), 611 (6.66). ^{1}H NMR (400 MHz, 20 °C) δ: 9.65 (s, 2H, CHO); 9.53 (s, 2H, β-H); 8.66 (d, 2H, $^3J_{HH}$ = 5.1 Hz, β-H); 8.58 (d, 2H, $^3J_{HH}$ = 5.1 Hz, β-H); 8.10 (m, 5H, 5,15-*o*-Ph + 10-*p*-Ph); 7.77 (m, 10H, 5,10,15-*m*-Ph + 10-*o*-Ph + 5,15-*p*-Ph). MS (ESI): M$^+$ = 776.1583 (expt), 776.1579 (calcd for $C_{39}H_{23}N_4O_2Au$). Elemental analysis (%) calcd for $C_{39}H_{23}N_4O_2Au$: C 60.32, H 2.99, N 7.21; found C 60.13, H 3.12, N 7.54.

Au[T*p*CH$_3$PC-3-CHO]. Yield 2.3 mg (11.3%). UV-vis (CH_2Cl_2) λ_{max} [nm, $\varepsilon \times 10^{-4}$ (M^{-1} cm^{-1})]: 428 (9.84), 581 (4.02), 602 (4.21). ^{1}H NMR (400 MHz, 20 °C) δ: 9.76 (s, 1H, CHO); 9.54 (s, 1H, β-H); 8.97 (d, 1H, $^3J_{HH}$ = 4.2 Hz, β-H); 8.90 (d, 1H, $^3J_{HH}$ = 4.9 Hz, β-H); 8.70 (d overlapping, 2H, $^3J_{HH}$ = 8.0 Hz, β-H); 8.64 (d overlapping, 2H, $^3J_{HH}$ = 4.8 Hz, β-H); 8.10 (d, 2H, $^3J_{HH}$ = 7.8 Hz, 10-*o*-Ph); 7.99 (d, 4H, $^3J_{HH}$ = 7.7 Hz, 5,15-*o*-Ph); 7.62 (d, 2H, $^3J_{HH}$ = 7.8 Hz, 10-*m*-Ph); 7.54 (dd, 4H, $^3J_{HH}$ = 12.6, 7.7 Hz, 5,15-*m*-Ph); 2.70 (s, 3H, *p*-CH_3), 2.68 (s, 6H, *p*-CH_3). MS (ESI): M$^+$ = 791.2080 (expt), 791.2079 (calcd for $C_{41}H_{29}N_4OAu$). Elemental analysis (%) calcd for $C_{41}H_{29}N_4OAu$: C 62.28, H 3.70, N 7.09; found C 62.53, H 3.62, N 7.43. IR ν_{CHO}: 1655 cm^{-1}.

Au[T*p*CH$_3$PC-3,17-(CHO)$_2$]. Yield 10.7 mg (53.5%). UV-vis (CH_2Cl_2) λ_{max} [nm, $\varepsilon \times 10^{-4}$ (M^{-1} cm^{-1})]: 425 (4.35), 439 (4.77), 596 (3.53), 615 (3.73). ^{1}H NMR (400 MHz, 20 °C) δ: 9.58 (s, 2H, CHO); 9.27 (s, 2H, β-H); 8.62 (d, 2H, $^3J_{HH}$ = 5.0 Hz, β-H); 8.56 (d, 2H, $^3J_{HH}$ = 5.1 Hz, β-H); 7.94 (d overlapping, 2H, $^3J_{HH}$ = 8.0 Hz, 10-*o*-Ph); 7.91 (d overlapping, 4H, $^3J_{HH}$ = 7.8 Hz, 5,15-*o*-Ph); 7.57 (d, 2H, $^3J_{HH}$ = 7.8 Hz, 10-*m*-Ph); 7.53 (d, 4H, $^3J_{HH}$ = 7.7 Hz, 5,15-*m*-Ph); 2.68 (s, 9H, *p*-CH_3). MS (ESI): M$^+$ = 819.2029 (expt), 818.2029 (calcd for $C_{42}H_{29}N_4O_2Au$). Elemental analysis (%) calcd for $C_{42}H_{29}N_4O_2Au$: C 61.62, H 3.57, N 6.84; found C 61.23, H 3.62, N 6.56. IR ν_{CHO}: 1663 cm^{-1}.

Au[T*p*OCH$_3$PC-3,17-(CHO)$_2$]. Yield 10.2 mg (51.1%). UV-vis (CH_2Cl_2) λ_{max} [nm, $\varepsilon \times 10^{-4}$ (M^{-1} cm^{-1})]: 426 (5.63), 439 (5.70), 597 (4.29), 618 (4.44). ^{1}H NMR (400 MHz, 20 °C, CD_2Cl_2)

δ: 9.70 (s, 2H, CHO); 9.35 (s, 2H, β-H); 8.67 (d, 2H, $^3J_{HH} = 5.0$ Hz, β-H); 8.60 (d, 2H, $^3J_{HH} = 5.0$ Hz, β-H); 7.99 (d broad, 6H, $^3J_{HH} = 8.0$ Hz, *m*-Ph); 7.32–7.27 (m, 6H, *o*-Ph); 4.08 (s, 6H, 5,15-*p*-OCH_3); 4.06 (s, 3H, 10-*p*-OCH_3). MS (ESI): $M^+ = 866.1806$ (expt), 866.1807 (calcd for $C_{42}H_{29}N_4O_5Au$). Elemental analysis (%) calcd for $C_{42}H_{29}N_4O_5Au$: C 58.21, H 3.37, N 6.46; found C 58.43, H 3.82, N 6.01.

Au[T*p*FPC-3-CHO]. Yield 4.1 mg (20.5%). UV-vis (CH_2Cl_2) λ_{max} [nm, $\varepsilon \times 10^{-4}$ (M^{-1} cm^{-1})]: 427 (7.02), 580 (2.75), 597 (2.53). ^{1}H NMR (20 °C, 400 MHz) δ: 9.68 (s, 1H, CHO); δ 9.42 (S, 1H, β-H); 8.86 (d, 1H, $^3J_{HH} = 4.5$ Hz, β-H); 8.80 (d, 1H, $^3J_{HH} = 4.9$ Hz, β-H); 8.59–8.55 (m, 4H, β-H); 8.11–8.07 (m, 2H, Ph-H); 8.00–7.94 (m, 4H, Ph-H); 7.47–7.34 (m, 6H, Ph-H). MS (ESI): $M^+ = 802.1257$ (expt), 802.1260 (calcd for $C_{38}H_{20}F_3N_4OAu$). Elemental analysis was not performed.

Au[T*p*FPC-3,17-(CHO)$_2$]. Yield 10 mg (52.8%). UV-vis (CH_2Cl_2): λ_{max} (nm), [$\varepsilon \times 10^{-4}$ (M^{-1} cm^{-1})]: 436 (6.53), 597 (4.29), 609 (4.91). ^{1}H NMR (400 MHz, $CDCl_3$, 20 °C) δ: 9.52 (s, 2H, CHO); 9.16 (s, 2H, β-H); 8-53-8.54 (d, 2H, $^3J_{HH} = 5.0$ Hz, β-H); 8.49 (d, 2H, $^3J_{HH} = 5.1$ Hz, β-H); 7.97–7.94 (m, 2H, Ph-H); 7.92–7.88 (m, 4H, Ph-H); 7.35–7.45 (m, 6H, Ph-H). MS (ESI): $M^+ = 830.1207$ (expt), 830.1209 (calcd for $C_{39}H_{20}F_3N_4O_2Au$). Elemental analysis (%) calcd for $C_{39}H_{29}F_3N_4O_2Au$: C 56.40, H 2.43, N 6.75; found: C 56.76, H 2.62, N 7.11.

X-ray crystallography

X-ray quality crystals were obtained *via* slow diffusion of methanol vapor into concentrated dichloromethane solutions of the compounds in question. X-ray data were collected (as previously described[37]) on beamline 12.2.1 at the Advanced Light Source, Lawrence Berkeley National Laboratory. Samples were mounted on MiTeGen Kapton loops and placed in a 100(2)-K nitrogen cold stream provided by an Oxford Cryostream 800 Plus low-temperature apparatus on the goniometer head of a Bruker D8 diffractometer equipped with a PHOTON II CPAD detector operating in shutterless mode. Diffraction data were collected using synchrotron radiation monochromated using silicon(111) to a wavelength of 0.7288(1)Å. An approximate full-sphere of data was collected using a combination of φ and ω scans with scan speeds of one second per degree for the φ scans and one and three seconds per degree for the ω scans at $2\theta = 0$ and $-20°$, respectively. The structures were solved by intrinsic phasing (SHELXT[50]) and refined by full-matrix least-squares on F^2 (SHELXL-2014 (ref. 51)). All non-hydrogen atoms were refined anisotropically. Hydrogen atoms were geometrically calculated and refined as riding atoms. Additional crystallographic information has been summarized in Table 1.

Conflicts of interest

There are no conflicts to declare.

Acknowledgements

This work was supported by the Research Council of Norway (grant no. 262229 and 324139 to AG) and the Arctic Center for Sustainable Energy at UiT – The Arctic University of Norway. The work also used resources of the Advanced Light Source, which is a DOE Office of Science User Facility under contract no. DE-AC02-05CH11231.

References

1 A. Ghosh, *Chem. Rev.*, 2017, **117**, 3798–3881.
2 S. Nardis, F. Mandoj, M. Stefanelli and R. Paolesse, *Coord. Chem. Rev.*, 2019, **388**, 360–405.
3 Y. Fang, Z. Ou and K. M. Kadish, *Chem. Rev.*, 2017, **117**, 3377–3419.
4 A. B. Alemayehu, K. E. Thomas and R. F. Einrem, *Acc. Chem. Res.*, 2021, **54**, 3095–3107.
5 A. B. Alemayehu and A. Ghosh, *J. Porphyrins Phthalocyanines*, 2011, **15**, 106–110.
6 E. Rabinovitch, I. Goldberg and Z. Gross, *Chem.–Eur. J*, 2011, **17**, 12294–12301.
7 K. E. Thomas, A. B. Alemayehu, J. Conradie, C. Beavers and A. Ghosh, *Inorg. Chem.*, 2011, **50**, 12844–12851.
8 R. F. Einrem, H. Braband, T. Fox, H. Vazquez-Lima, R. Alberto and A. Ghosh, *Chem.–Eur. J*, 2016, **22**, 18747–18751.
9 R. F. Einrem, K. J. Gagnon, A. B. Alemayehu and A. Ghosh, *Chem.–Eur. J*, 2016, **22**, 517–520.
10 A. B. Alemayehu, S. J. Teat, S. M. Borisov and A. Ghosh, *Inorg. Chem.*, 2020, **59**, 6382–6389.
11 A. B. Alemayehu, H. Vazquez-Lima, K. J. Gagnon and A. Ghosh, *Inorg. Chem.*, 2017, **56**, 5285–5294.
12 A. B. Alemayehu, K. J. Gagnon, J. Terner and A. Ghosh, *Angew. Chem., Int. Ed.*, 2014, **53**, 14411–14414.
13 A. B. Alemayehu, H. Vazquez-Lima, C. M. Beavers, K. J. Gagnon, J. Bendix and A. Ghosh, *Chem. Commun.*, 2014, **50**, 11093–11096.
14 A. B. Alemayehu, L. J. McCormick, K. J. Gagnon, S. M. Borisov and A. Ghosh, *ACS Omega*, 2018, **3**, 9360–9368.
15 A. B. Alemayehu, H. Vazquez-Lima, K. J. Gagnon and A. Ghosh, *Chem.–Eur. J*, 2016, **22**, 6914–6920.
16 A. B. Alemayehu, H. Vazquez-Lima, L. J. McCormick and A. Ghosh, *Chem. Commun.*, 2017, **53**, 5830–5833.
17 C. Schies, A. B. Alemayehu, H. Vazquez-Lima, K. E. Thomas, T. Bruhn, G. Bringmann and A. Ghosh, *Chem. Commun.*, 2017, **53**, 6121–6124.
18 A. B. Alemayehu, L. J. McCormick-McPherson, J. Conradie and A. Ghosh, *Inorg. Chem.*, 2021, **60**, 8315–8321.
19 J. H. Palmer, A. C. Durrell, Z. Gross, J. R. Winkler and H. B. Gray, *J. Am. Chem. Soc.*, 2010, **132**, 9230–9231.
20 W. Sinha, L. Ravotto, P. Ceroni and S. Kar, *Dalton Trans.*, 2015, **44**, 17767–17773.
21 S. M. Borisov, A. B. Alemayehu and A. Ghosh, *J. Mater. Chem. C*, 2016, **4**, 5822–5828.
22 C. M. Lemon, D. C. Powers, P. J. Brothers and D. G. Nocera, *Inorg. Chem.*, 2017, **56**, 10991–10997.
23 A. B. Alemayehu, N. U. Jae Day, T. Mani, A. B. Rudine, K. E. Thomas, O. A. Gederaas, S. A. Vinogradov, C. C. Wamser and A. Ghosh, *ACS Appl. Mater. Interfaces*, 2016, **8**, 18935–18942.

24 S. M. Borisov, R. F. Einrem, A. B. Alemayehu and A. Ghosh, *Photochem. Photobiol. Sci.*, 2019, **18**, 1166–1170.
25 R. D. Teo, J. Y. Hwang, J. Termini, Z. Gross and H. B. Gray, *Chem. Rev.*, 2017, **117**, 2711–2729.
26 A. Mahammed and Z. Gross, *Coord. Chem. Rev.*, 2019, **379**, 121–132.
27 C. M. Lemon, *Pure Appl. Chem.*, 2020, **92**, 1901–1919.
28 G. Golubkov, *et al.*, *Angew. Chem., Int. Ed.*, 2001, **40**, 2132–2134.
29 J. F. B. Barata, M. G. P. M. S. Neves, M. A. F. Fautino, A. C. Tomé and J. A. Cavaleiro, *Chem. Rev.*, 2017, **117**, 3192–3253.
30 J. H. Palmer, A. C. Durrell, Z. Gross, J. R. Winkler and H. B. Gray, *J. Am. Chem. Soc.*, 2008, **130**, 7786–7787.
31 K. E. Thomas, J. Conradie, L. K. Hansen and A. Ghosh, *Eur. J. Inorg. Chem.*, 2011, 1865–1870.
32 S. Berg, K. E. Thomas, C. M. Beavers and A. Ghosh, *Inorg. Chem.*, 2012, **51**, 9911–9916.
33 K. E. Thomas, L. J. McCormick, D. Carrié, H. Vazquez-Lima, G. Simmoneaux and A. Ghosh, *Inorg. Chem.*, 2018, **57**, 4270–4276.
34 I. K. Thomassen, L. J. McCormick and A. Ghosh, *ACS Omega*, 2018, **3**, 5106–5110.
35 A. Reinholdt, A. B. Alemayehu, K. J. Gagnon, J. Bendix and A. Ghosh, *Inorg. Chem.*, 2020, **59**, 5276–5280.
36 J. H. Palmer, A. C. Durrell, Z. Gross, J. R. Winkler and H. B. Gray, *J. Am. Chem. Soc.*, 2008, **130**, 7786–7787.
37 A. B. Alemayehu, R. F. Einrem, L. J. McCormick-McPherson, N. S. Settineri and A. Ghosh, *Sci. Rep.*, 2020, **10**, 19727.
38 M. Soll, *et al.*, *Org. Lett.*, 2016, **18**, 5840–5843.
39 K. Sudhakar, *et al.*, *Angew. Chem., Int. Ed.*, 2017, **56**, 9837–9841.
40 P. Schweyen, K. Brandhorst, M. Hoffmann, B. Wolfram, M.-K. Zaretzke and M. Bröring, *Chem.–Eur. J*, 2017, **23**, 13897–13900.
41 H. Vazquez-Lima, J. Conradie, M. A. L. Johansen, S. R. Martinsen, A. B. Alemayehu and A. Ghosh, *Dalton Trans.*, 2021, **50**, 12843–12849.
42 I. K. Thomassen, D. Rasmussen, R. F. Einrem and A. Ghosh, *ACS Omega*, 2021, **6**, 16683–16687.
43 A. Vilsmeier and A. Haack, *Ber. Dtsch. Chem. Ges.*, 1927, **27**, 119–122, DOI: 10.1002/cber.19270600118.
44 R. Paolesse, L. Jaquinod, M. O. Senge and K. M. Smith, *J. Org. Chem.*, 1997, **62**, 6193–6198.
45 I. Saltsman, A. Mahammed, I. Goldberg, E. Tkachenko, M. Botoshansky and Z. Gross, *J. Am. Chem. Soc.*, 2002, **124**, 7411–7420.
46 R. Paolesse, S. Nardis, M. Venanzi, M. Mastroianni, M. Russo, F. Fronczek and M. G. H. Vicente, *Chem.–Eur. J*, 2003, **9**, 1192–1197.
47 K. Sorasaenee, P. Taqavi, L. M. Henling, H. B. Gray, E. Tkachenko, A. Mahammed and Z. Gross, *J. Porphyrins Phthalocyanines*, 2007, **11**, 189–197.
48 S. Ganguly and A. Ghosh, *Acc. Chem. Res.*, 2019, **52**, 2003–2014.
49 J.-H. Fuhrhop, K. M. Kadish and D. G. Davis, *J. Am. Chem. Soc.*, 1973, **95**, 5140–5147.
50 G. M. Sheldrick, *Acta Crystallogr., Sect. A: Found. Crystallogr.*, 2015, **71**, 3–8.
51 G. M. Sheldrick, *Acta Crystallogr., Sect. C: Struct. Chem.*, 2015, **71**, 3–8.